Analysis of Notched Newsprint Sheet in Mode I Fracture

J. TRYDING and P.J. GUSTAFSSON

A new approach to analyze notched paper sheet loaded in mode I, based on cohesive crack modelling, is investigated. The method predicts final failure of the sheet, regardless of the sheet size and initial crack length. Onset of crack growth, stable crack growth and onset of unstable crack growth are predicted. The simulations of the notched paper sheet reveal that the concept of autonomy, i.e. independence of specimen geometry and load configuration, in a region near the crack edge does not in general prevail, except at small-scale yielding. The method is confirmed by a large number of experimental tests. Different sheet sizes are tested. In the experiments, 45 g/m² newsprint was used.

Nous avons étudié une nouvelle technique permettant d'analyser une feuille de papier encochée chargée en mode I, en se basant sur la modélisation cohésive des craquelures. La méthode prévoit la défaillance finale de la feuille, peu importe sa dimension ou la longueur initiale de la craquelure. Le commencement de la craquelure, le développement de la stabilité de la craquelure et le commencement de l'instabilité de la craquelure sont prévus. Les simulations de la feuille de papier encochée révèlent que le concept d'autonomie, c'est-à-dire l'indépendance de la géométrie du spécimen et de la configuration des charges, dans une zone près du bord de la craquelure, n'est pas en général prédominant, sauf lors d'une moindre résistance. La méthode est confirmée par un bon nombre d'essais. Des feuilles de diverses dimensions sont soumises à l'essai. Pour ces essais, du papier journal de 45 g/m² a été utilisé.

INTRODUCTION

Notched paper sheets loaded in-plane in mode I, regardless of size, fails through fracture. The region where fracture takes place near the crack edge is called the process region [1,2]. The loads in the process region are so high that the wood fibres, linked together fibre-to-fibre, debonds [3,4]. Further loading results in pull-out of single fibre bridges until the separation is complete [5]. The separation that occurs in the process region is described here by a cohesive crack type of approach [6–8], intended to characterize the fracture in paper near the crack edge. The cohesive crack model is characterized by a relation between the descending stress and the crack widening during failure of the paper [9,10]. The stress-crack widening curve is obtained from tests of uniaxial loaded paper strips without any pre-existing crack. To record a stable descending load-elongation curve, from which the stress-crack widening curve is obtained, the paper strip must be short and the test equipment stiff. The fracture energy needed to separate the fracture surfaces is defined as the area under the stress-crack widening curve [8].

Cohesive crack models are frequently and successfully used to characterize the fracture in brittle and quasi-brittle material such as, for example, concrete [7,11], fibre-reinforced plastic and laminates [12,13], wood [14] and wood adhesive joints [15].

Cohesive crack models are fundamentally different from the classical fracture mechanics models, where the theory is based on a critical quantity that controls the onset of growth of a pre-existing sharp crack [16–18]. The critical quantity is expressed by, for example, the stress intensity factor, the energy release rate, the J integral or the crack opening displacement. The classical fracture mechanics models can in general be expected to give good results if the size of the fracture process region is very small compared to the length of the crack and the ligament. The applicability of cohesive crack models is, in several senses, more general. The fracture properties of the material are defined in a more complete manner and there are no presumptions regarding the size (the complete length) of the fracture region or regarding existence of a crack. One reason why cohesive crack models have become an object for major research and application only in recent decades might be that applied analysis in general requires use of a computer with a good capacity for numerical calculations, e.g. by the finite element method.

This article concerns the analysis of a rectangular sheet $2W$ wide and $2H$ high containing a central crack $2a$ long where the ends of the sheet are subjected to uniform displacement perpendicular to the crack line and zero displacement parallel to the crack line (Fig. 1). Experimental observations of the central cracked rectangular sheet (CCS) are discussed in this paper and experiments and simulations of the CCS are compared, when the MD is perpendicular to the crack line. Newsprint (45 g/m²) is used in the experiments and an elastic-cohesive softening (ECS) model [9] calibrated to the newsprint

J. Tryding
AssiDomän AB
SE-617 10 Skärblacka, Sweden
(johan.tryding@asdo.se)
P.J. Gustafsson
Div. Structural Mechanics
Lund University
Box 118
SE-221 00 Lund, Sweden

is used in the simulations. The process region just ahead of the crack tip and its influence on the overall load-deformation relation are analyzed in the last sections of this paper.

CENTRAL CRACKED SHEET IN MODE I

In the literature, a considerable amount of work is presented on experiments, theories and analysis of notched paper specimens [19–30]. In this paper, two heights of the CCS are studied, one of a height shorter than the critical paper strip length (i.e. $2H = 10$ mm), and one of a height greater than the critical length ($2H$ = 100 mm). The width is equal to $2W = 50$ mm and the crack length $2a = 20$ mm. The critical length is defined as the shortest length of an un-notched paper strip for which the load-elongation curve (in stroke-controlled testing by a stiff testing device) immediately falls from a point of instability to zero [31]. For newsprint the measured critical length is 35 mm in MD and 65 mm in CD [9].

The tests were made at a relative humidity of 50 ± 2% and at a temperature of 23 ± 1°C. The CCS specimens were held by pneumatic vice-action grips between two parallel textured jaw faces. The constant rate of the elongation for a test span $2H$ is adjusted to give the same strain rate, i.e. stroke rate of $0.1H$ mm/min. The initial crack in the CCS was obtained by a scalpel. The material used in the experiments is 45 g/m^2 newsprint. The sheet thickness was measured by a Lorentzen & Wettre thickness tester to be 72 μm (mean value). At least six nominally equal tests were made for each height.

EXPERIMENTAL OBSERVATIONS

The experimentally obtained load-deformation curves for the CCS specimens of heights 100 mm and 10 mm loaded in the MD are shown in Figs. 2 and 3, respectively. The 6 dashed curves in Figs. 2 and 3 are replicate determinations of the experimental load-elongation curve. In Figs. 2 and 3, the compliance of the loadcell has been subtracted from the recorded elongations. It is seen from comparison of Figs. 2 and 3 that the shorter CCS specimen ($2H$ = 10 mm) exhibits a stable descending load-displacement curve, which is a measure of a stable process region (localized damage) growth throughout the ligament length. The long CCS specimen ($2H$ = 100 mm) exhibits immediate rupture, i.e. unstable process region growth.

Different limit loads (maximum load) are observed for the long and short CCS specimens (cf. Figs. 2, 3). For the long CCS in Fig. 2 the limit load ranges from 43 to 47 N, and for the short CCS in Fig. 3 the limit load ranges from 54 to 64 N (if the lowest curve is excluded in Fig. 3), i.e. the limit load for the short CCS is larger than for the long CCS. Comparison between Figs. 2 and 3 shows that the initial stiffness for the long CCS is less than for the short CCS. However, if the initial stiffness is divided by the cross-section area, $A = (2W–2a)t$, and multiplied by the length of the specimen, $2H$, i.e. $(F/A)/(u/2H)$, then it is found that $(F/A)/(u/2H)$ for the long CCS (~6.3 GPa) is greater than for the short CCS (~4.8 GPa). Thus the limit load decreases and the normalized initial stiffness defined as $(F/A)/(u/2H)$ increases with increasing height.

In Figs. 4 and 5, the crack path is shown for the long and short CCS loaded in the MD. It is seen in Fig. 4 that the crack paths for a typical long CCS are approximately parallel with the pre-existing crack. Figure 5 shows the crack paths for the short CCS. It is seen that some crack paths are parallel to the pre-existing crack, whereas some divert considerably from a plane parallel to the pre-existing crack. The scatter in the limit load for the short CCS as compared to the long CCS for loading in the MD (cf. Figs. 2, 3) is assumed to depend on the scatter in the crack path observed in Fig. 5 for the short CCS.

OUTLINE OF THE ECS MATERIAL MODEL

The ECS model consists of an orthotropic linear elastic model up to a failure criterion is reached. Thereafter localized fracture softening with a gradually decreasing stress at increasing localized deformation is assumed to take place. The orthotropic

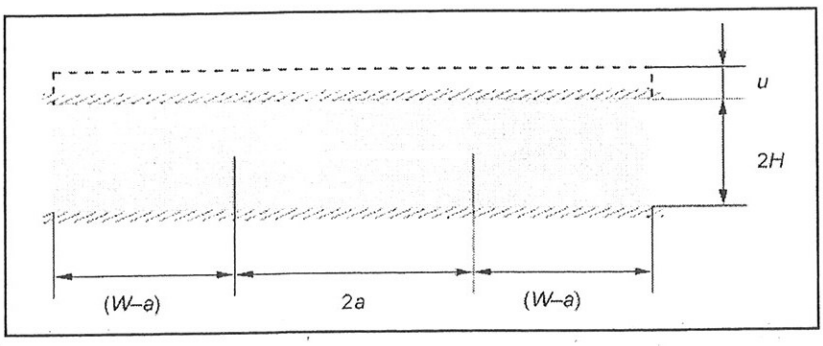

Fig. 1. The CCS geometry.

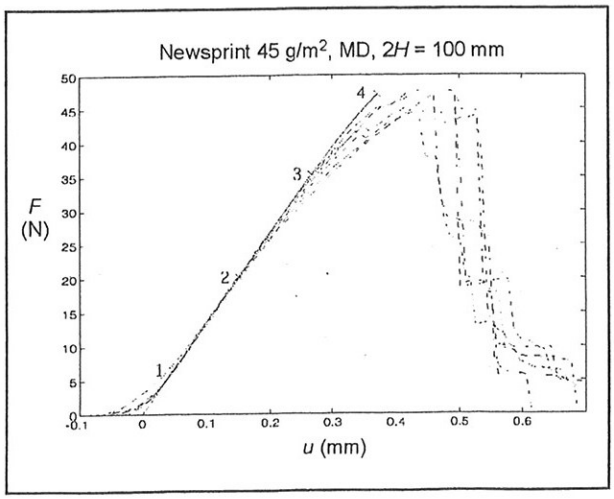

Fig. 2. The load-elongation curves from experiments (dashed lines) and simulation with the ECS model (solid line) for the long CCS loaded in the MD.

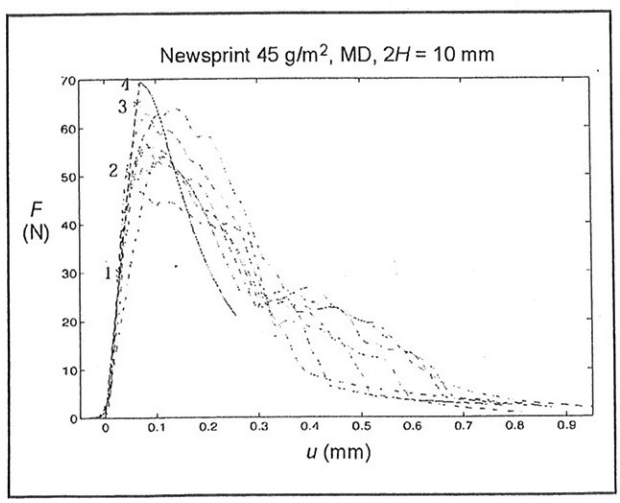

Fig. 3. The load-elongation curves from experiments (dashed lines) and simulation with the ECS model (solid line) for the short CCS loaded in the MD.

Fig. 4. Typical long CCS specimens loaded in the MD.

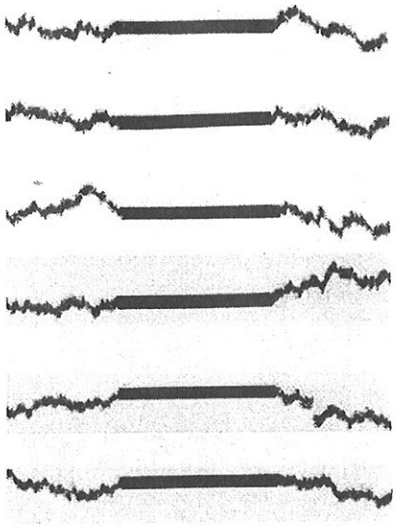

Fig. 5. The short CCS specimens loaded in the MD.

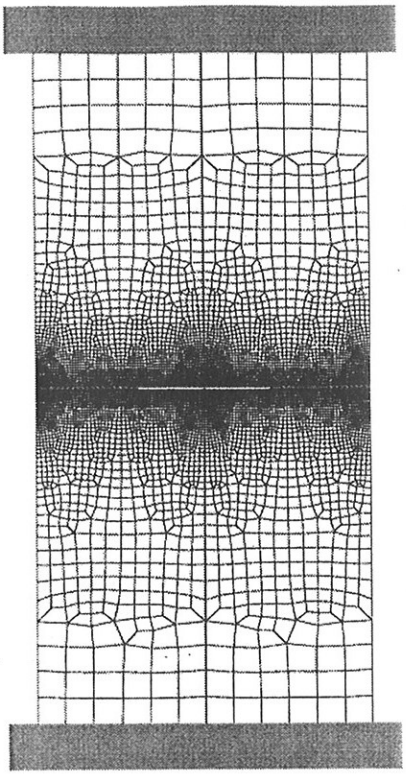

Fig. 6. The numbers of elements and nodes in half of the mesh are 4195 and 4341, respectively. The elements ahead of the crack edge are quadratic with a side length of 0.25 mm.

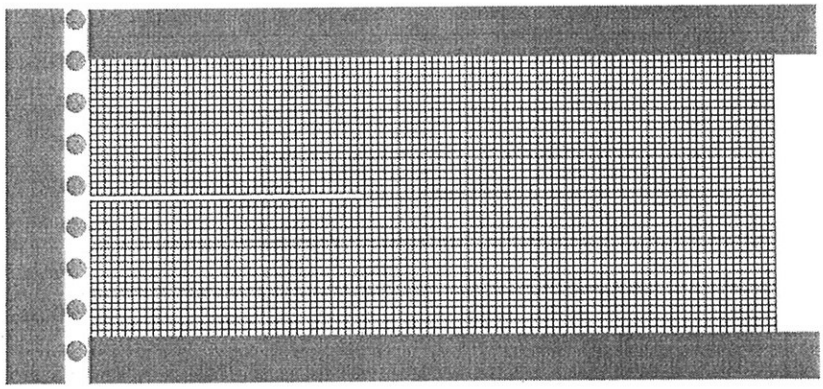

Fig. 7. The numbers of elements and nodes in the mesh are 4019 and 4200, respectively. The elements ahead of the crack edge are quadratic with a side length of 0.2439 mm.

elastic properties are defined by E_1, E_2, ν_{12}, and G_6. The failure criterion used is the Hill-Tsai-Wu criterion [32,9], defined by the in-plane tensile strengths, T_1^0, T_2^0, the shear strength, T_6^0, the compressive strengths, C_1^0, C_2^0, and the equibiaxial tensile strength, P. The subindexes 1, 2 and 6 denote the MD, CD and in-plane shear, respectively. The stress rate in the fracture softening stage is related to the crack opening rate according to an orthotropic nonassociated fracture rule. The parameters defining this rule are determined from stable tensile tests of un-notched paper strips [10]. A thorough detailed description of the ECS model and its numerical implementation is found in Tryding's Ph.D. thesis [9].

COMPARISON WITH FINITE ELEMENT SIMULATIONS

The finite element mesh used in the simulations of the CCS specimens is shown in Fig. 6 ($2H$ = 100 mm) and Fig. 7 ($2H$ = 10 mm). In the simulations, half of the geometry is used, due to symmetry reasons, for both the long and short CCS. The boundary conditions on the geometries are the ones shown in Figs. 6 and 7. The mesh in Figs. 6 and 7 consists of four node plane stress elements. It is assumed in the simulations that the process region ahead of the crack tip grows in the direction of the pre-existing crack. Reduced integration is used for the four-node element row straight ahead of the pre-existing crack. The elements in the ligament length (the distance W–a in Fig. 1) are given the ECS model material property [9], and all other elements in the mesh are given orthotropic elastic material properties.

The ECS material model is calibrated to 45 g/m^2 newsprint material data (see Tables I, II, Fig. 8; cf. [9]). Figure 8 shows the experimental results obtained for the newsprint from uniaxial in-plane tension in the MD of specimens 72 μm thick, 5 mm long between the grips and 15 mm wide. This specimen is considered in a finite element analysis. The results from the

TABLE I
ELASTIC CONSTANTS (MEAN VALUES)

E_1 [MPa]	4560
E_2 [MPa]	873
ν_{12}	0.31
G_6 [MPa]	879

TABLE II
COHESIVE SOFTENING PARAMETERS (MEAN VALUES)

T_1^0 [MPa]	C_1^0 [MPa]	T_2^0 [MPa]	C_2^0 [MPa]	T_6^0 [MPa]	P^0 [MPa]
31.9	15.3	10.8	5.56	7.8	11.9

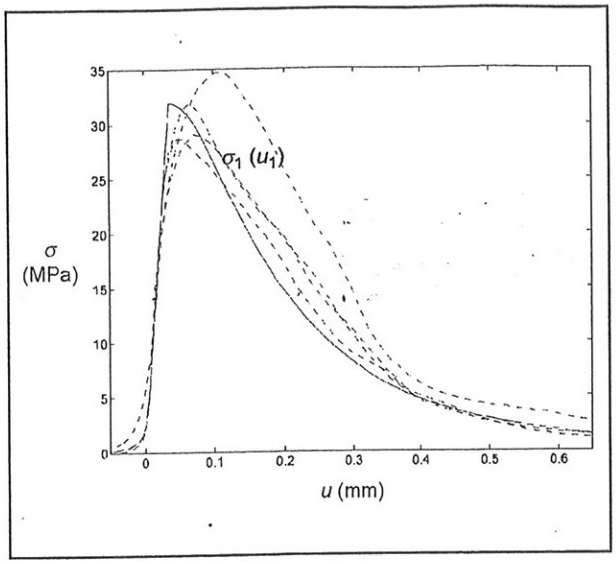

Fig. 8. Experimental replicate determinations (dashed lines) and simulated (solid line) uniaxial load-elongation curves for the short newsprint strip.

simulation with 24 × 8 four-node elements with reduced integration are shown in Fig. 8 together with experiment results. The agreement with the ascending part of the stress-elongation in Fig. 8 is good, even if the influence of the plastic part in the MD is not taken into consideration.

Simulations of the CCS specimens loaded in the MD are shown in Figs. 2 and 3, where the simulation of the CCS specimen is plotted together with the experiments. It is seen that good agreement is obtained between the simulations and experiments. From this it can be assumed that the plastic effects in MD are small in comparison with the elastic and cohesive softening effects, which justifies the choice of the ECS model in the simulations. The prediction of the limit load for the long CCS specimen is in good agreement with the measured results, whereas the short CCS specimen overpredicts the limit load in the range of 9–22% (cf. Figs. 2, 3).

Figures 9 and 11 show the stress in the loading direction (MD) normalized with the failure stress in the MD, σ_1/T_1^0, ahead of the crack tips for the long and short CCS specimens, respectively, plotted against the width, $2W$, of the CCS geometry. Figures 10 and 12 show the stress in the transverse loading direction normalized with the failure stress in the CD, σ_2/T_2^0, ahead of the crack tips for the long and short CCS specimens, respectively, plotted against the width, $2W$, of the CCS geometry. The stress curves in Figs. 9–12 are obtained from the

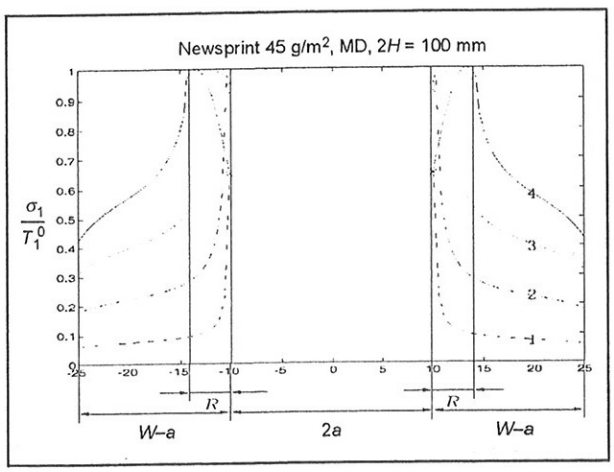

Fig. 9. Calculated normalized stress, σ_1/T_1^0, versus the width, $2W$, of the long CCS geometry.

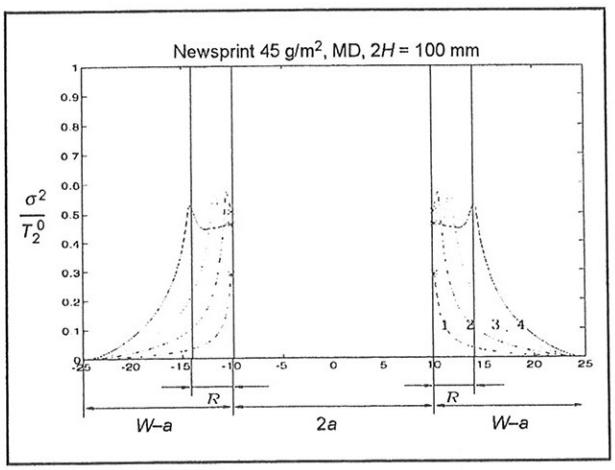

Fig. 10. Calculated normalized stress, σ_2/T_2^0, versus the width, $2W$, of the long CCS geometry.

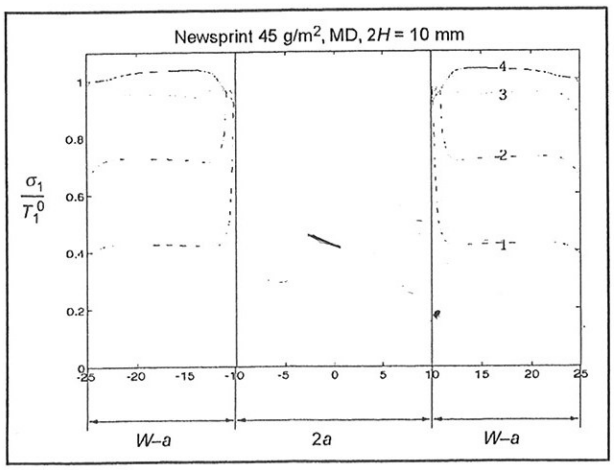

Fig. 11. Calculated normalized stress, σ_1/T_1^0, versus the width, $2W$, of the short CCS geometry.

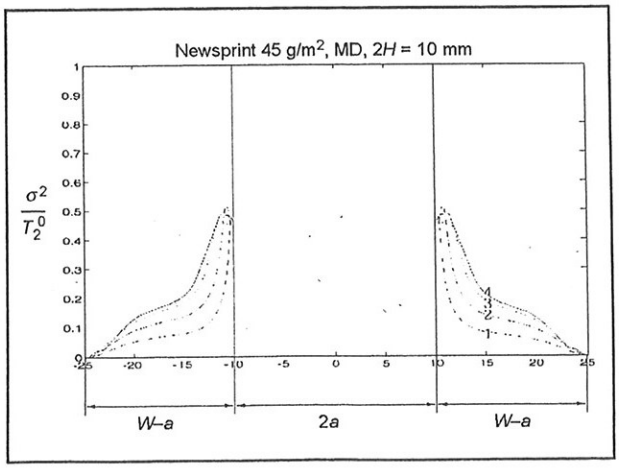

Fig. 12. Calculated normalized stress, σ_2/T_2^0, versus the width, $2W$, of the short CCS geometry.

loads referred to as 1, 2, 3 and 4 in Figs. 2 and 3. The 'x' in Figs. 9 and 10 denotes the stresses at the Gauss point in the element at the crack tip for the stress curves referred to as 1, 2, 3 and 4. The shear stress is equal to zero in the ligament length ahead of the crack tip, so the stresses, σ_1 and σ_2 are equal to the principal stresses.

For the long CCS specimen, the extent of the process region ahead of the crack tip is given at the maximum normalized stress, σ_2/T_2^0 in Fig. 10, for the loads referred to as numbers 1 to 4 in Fig. 2. This is illustrated by R in Figs. 9 and 10 for the stresses referred to as number 4.

The numbered loads are denoted as F_i, where i is equal to numbers 1, 2, 3 and 4 in Fig. 2. It is seen from Fig. 10 that the growth of the process region from the load, $F = 0$ to $F_3 \cong 0.73F_{limit}$, where $F_{limit} = 47.1$ N is limit load, is approximately the same as the growth of the process region from $F_3 \cong 0.73F_{limit}$ to $F_4 = F_{limit}$. The normalized stress, σ_1/T_1^0, at the crack tip is non-zero during the ascending part of the load-elongation curve (cf. Figs. 2, 9). This implies that the process region grows during the ascending part, i.e. no crack growth occurs during the ascending part. After the limit load is reached, the process region grows unstable until the end of the ligament is reached, i.e. $R = (W-a) = 15$ mm.

For the short CCS specimen, the process region is $R \cong 2.1$ mm at the load, $F_3 \cong 0.94F_{limit}$, where $F_{limit} = 69.5$ N, and at the limit load $F_4 = F_{limit}$ the process region is $R <\cong 15$ mm, i.e. the process region near the limit load grows stable from a process region of $R \cong 2.1$ mm to $R <\cong 15$ mm.

The simulations in Figs. 9–12 reveal that, at the same reaction force, the extent of the process region ahead of the crack tip, R, for the long CCS has extended much more into the ligament length as compared to the short CCS specimen. This observation reveals the fact that the concentration of the stresses at the crack tip, at the same remote loading, is more pronounced for the long CCS than for the short CCS. From comparison at loads near the limit load in Figs. 9 and 11, it is seen that the stress curve in the loading direction for the long CCS is more concentrated in the process region, whereas for the short CCS the stress curve is more or less the same over the ligament length $(W-a)$. It should further be noted that, in the end of the process region, the stresses in the loading direction and the stresses in the transverse loading direction have the following relation $\sigma_2/T_2^0 \cong 0.5\ \sigma_1/T_1^0$.

In Fig. 13 are shown the principal stresses close to the limit load for the long CCS specimen. It is seen in the lower figure that the principal compressive stresses arise at the boundary of the pre-existing crack and that the principal compressive stresses surround the ligament length. The principal compression stresses may give out-of-plane movements; this implies that anti-buckling guides should be used in the experiments to get a better agreement between the experiments and the simulations. It is further seen in Fig. 13 (upper figure) that the stresses are concentrated around the process region tip and the stresses decrease in the process region (see also Figs. 9–12).

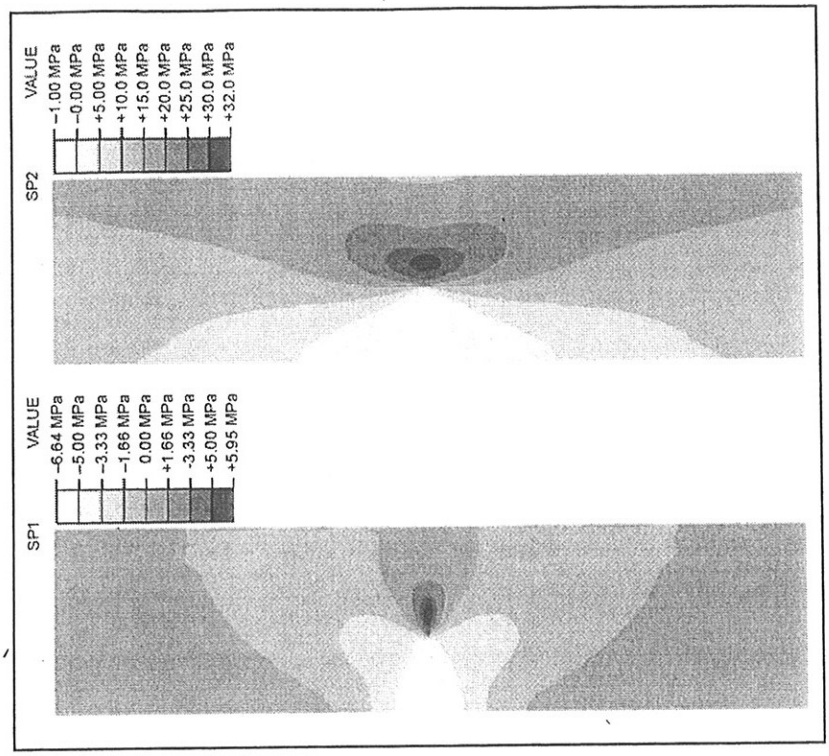

Fig. 13. The principal stresses for the long CCS loaded in the MD.

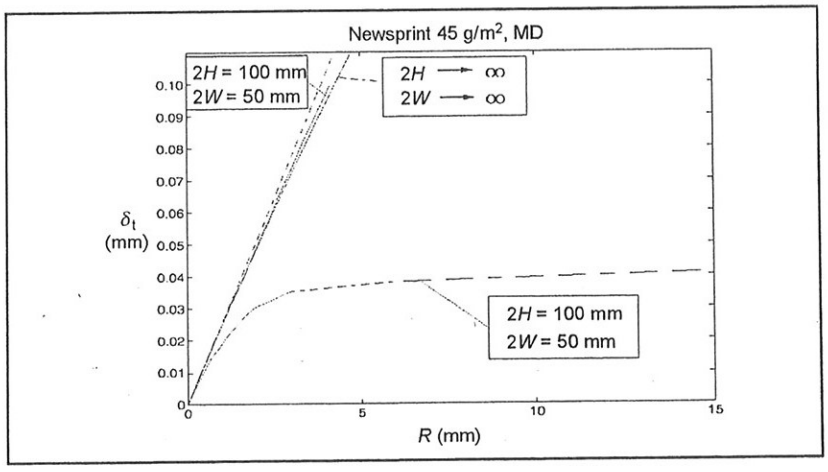

Fig. 14. The crack opening displacement (COD), δ_t, versus the extent of the process region of the crack tip, R, into the ligament length.

PROCESS REGION AHEAD OF THE CRACK TIP

From the simulations of the short and the long CCS specimens loaded in the MD, it is interesting to notice that the crack-opening displacement (COD), δ_t, versus the extent of the process region ahead of the crack tip, R, is initially the same, cf. Fig. 14. So initially the same fracture process occurs at the crack tip independently of body geometry, i.e. we have the concept of near-edge autonomy. The definition of near-edge autonomy is that the same events occur near the crack edge in the material, irrespective of structure geometry and load configuration [6,33]. It should be pointed out that conventional methods in fracture mechanics rest on the assumption of autonomy in the region near the crack tip [34]. So the process region can uniquely be described by one parameter only, irrespective of structure geometry and load configuration. Often the J integral is chosen for this purpose, i.e. the

measure of the fracture energy dissipation to the crack tip. However, it is shown from Fig. 14 that when the localized damage zone ahead of the crack tip has extended approximately 3% into the total ligament length $(W-a)$ = 15 mm, i.e. $R/(W-a)$ = 0.03, the short and long specimens give different δt vs R response. This means that the concept of autonomy in a region near the crack edge no longer prevails, and the process region near the crack edge therefore cannot generally be described by one unique parameter.

The deviation from autonomy is considerable at peak load, both for the long and short CCS. At peak load for $2H$ = 100 mm, the opening displacement is $\delta_t \cong 0.1$ mm, and the extent of the process region of the crack tip, $R \cong 4.1$ mm. And at peak load for $2H$ = 10 mm, $\delta_t \cong 0.04$ mm and $R \cong 15$ mm.

The simulated results of the process region just ahead of the crack tip are compared with the analytical solution of an infinite cracked plate in tension, i.e. the Barenblatt-Dugdale crack model. The infinite cracked plate problem has been solved and discussed in detail by Andersson and Bergkvist [7] and Rice [18].

$$\delta_t = \frac{8\sigma_y a}{\pi E}\ln\left[\sec\left(\frac{\pi\sigma_\infty}{2\sigma_y}\right)\right] = \frac{\pi\sigma_\infty^2 a}{E\sigma_y} + \ldots \quad (1)$$

They investigated an infinite cracked plate loaded with a uniform remote stress, σ_∞, under plane stress condition with a crack $2a$ long. Andersson and Bergkvist [7] studied an isotropic linear elastic material with a descending stress-elongation curve. Rice [18] used an isotropic linear elastic material with nonhardening plasticity. The solution of the nonhardening model for large-scale yielding (LSY) gives the crack opening displacement, δ_t, and the maximal extent of the yielding ahead of the crack tip, R (cf. [18]),

$$R = a\left[\sec\left(\frac{\pi\sigma_\infty}{2\sigma_y}\right) - 1\right] = \frac{\pi}{8}\left(\frac{\sigma_\infty}{\sigma_y}\right)^2 a + \ldots \quad (2)$$

where σ_y is the yield stress and E is the elastic modules in an anisotropic material.

A combination of Eqs. (1) and (2) gives the relationship between the crack opening displacement, δ_t, and the extent of the yielding zone ahead of the crack tip, R, as

$$\delta_t = \kappa a \ln\left[\frac{R}{a} + 1\right] = \kappa R + \ldots \quad (3)$$

where κ is equal to $8/\pi\cdot\sigma_y/E$. The first terms in the Taylor expansion in Eqs. (1)–(3) are the results obtained at small-scale yielding (SSY) for plane stress condition.

The relationship between the COD, δ_t, and the extent of the yielding zone ahead of the crack tip, R, in Eq. (3) is plotted in Fig. 14 for both LSY ($2H \to \infty$ and $2W \to \infty$) and SSY (dashed line), for κ = 0.0257. The value of κ was obtained from simulations of large CCS specimens loaded in the MD. In Fig. 14, it is shown that the simulated δ_t–R curve for the long CCS specimen and the LSY relation in Eq. (3) with κ = 0.0257 gives nearly the same result. It is further seen that the SSY solution deviates only slightly from the LSY solution in Fig. 14 before instability occurs, i.e. at $R \cong 4.1$ mm.

LIMIT LOAD ESTIMATION

The limit loads derived from the simulations above are shown in Table III together with the experiments. If it is assumed that the length of the process region at the limit load is either zero, i.e. a point, or equal to the ligament length $(W-a)$, then a simple estimate of the limit load can be made.

Let us first assume that the process region is point sized at the crack tip. Then linear elastic fracture mechanic (LEFM) methods can be used to establish an estimate of the limit load. The CCS specimens are subjected to uniform displacement perpendicular to the crack line, u. The constitutive relation between the reaction force, F, and the displacement, u, is

$$u = S(A)F \quad (4)$$

where $S(A)$ is the compliance stiffness (inverse elastic stiffness) given in Figs. 2–3 and $A = (2W-2a)t$ is the CCS cross-section area. The strain energy under the prescribed displacement, u, is

$$U = \frac{1}{2}uF = \frac{1}{2}S(A)F^2 \quad (5)$$

where Eq. (4) has been applied.

Assume next that the crack grows from its initial length, $2a$, to a new crack length, $2(a + \delta a)$. This means that fracture energy has been dissipated in the point-sized process region with the result that new crack surfaces have been generated, i.e. $t2\delta a$, where t is the CCS thickness. The loss of potential elastic-strain energy per unit area due to generated fracture surface was assumed by Griffith to be equal to the released elastic energy [16]. However, much larger energy is dissipated and Orowan [35] extended Griffith's theory to include the whole energy dissipation, i.e.

$$\frac{dU}{dA} \equiv G_f \quad (6)$$

where G_f is the fracture energy (cf. [10]). The results in Eq. (6) hold only for SSY [36]. Differentiation of Eq. (5) with respect to the area, A, gives the loss of potential elastic-strain energy per unit area as

$$\frac{dU}{dA} = \frac{1}{2}F^2\frac{dS(A)}{dA} \quad (7)$$

The LEFM estimate of the limit load is then given by insertion of Eq. (6) into Eq. (7) and, after some rearrangements, gives [37],

$$F_{limit}^{LEFM} = \sqrt{2G_f\left(\frac{dS}{dA}\right)^{-1}} \quad (8)$$

where the changes in the compliance stiffness with respect to creation of new crack surface, dS/dA, are obtained from linear orthotropic elastic finite element simulations of the long and short CCS with different crack length $2a$, i.e. $2a$ = 20, 21 and 22 mm. In Table III the LEFM limit loads are given for the short and long CCS specimens loaded in the MD. The fracture energy values for newsprint 45 g/m^2 is 7.10 kJ/m^2 in the MD (cf. [9]).

If the process region is equal to the ligament length $(W-a)$ and it is assumed that the stress in the loading direction over the ligament length is equal to the failure stress, T_1^0, then a simple estimate of the limit load can be made as

$$F_{limit}^{Failure} = T_1^0(2W - 2a)\cdot t \quad (9)$$

In Table III the failure stress limit loads are given for the short and long CCS specimens. The failure stress values for 45 g/m^2 newsprint is T_1^0 = 31.9 MPa in the MD.

All estimates of the limit load in Table III are shown to overestimate the experimental results. It is seen that the simulations with the cohesive softening model give good or reasonable predictions of the experimentally obtained limit loads. The prediction by the estimated form the failures stress in Eq. (9) is shown to be in agreement for the short CCS, whereas it overestimates the long CCS loaded in the MD by approximately 50%. The good estimate for the short CCS may be because the principal stresses are more or less constant in the loading direction along the ligament length at the limit load (cf. Fig. 11). The LEFM limit load estimates are shown in Table III to overestimate both of the experimentally obtained limit loads considerably.

TABLE III
LIMIT LOADS

	LEFM	Failure stress	Simulations	Experiments
$2H$ [mm]	F_{limit}^{LEFM} [N]	$F_{limit}^{Failure}$ [N]	F_{limit}^{ECR} [N]	F_{limit}^{Exp} [N]
10	177	68.9	69.5	54 – 64
100	83	68.9	47.1	43 – 47

SUMMARY

A rectangular sheet containing a central crack is analyzed in order to investigate how well the developed model is able to describe experimental observations. It is found that the limit loads and size effects are picked up very well by the developed model. The size of the fractured process region is found to be very large compared to the length of the crack and the ligament.

The simulations of the CCS specimen reveal that the concept of autonomy in a region near the crack edge does not in general prevail, except at SSY, since the crack opening displacement, δ_t, versus the extent of the process region ahead of the crack tip, R, gives different curve response for the short and long CCS specimen. So, the process region near the crack edge can therefore not generally be described by only one unique parameter, e.g. the J integral.

ACKNOWLEDGEMENTS

The authors would like to thank Dr. Bengt Carlsson and Professor Hans Petersson for many valuable discussions, comments and suggestions during the work. Financial support from Tetra Pak and the Swedish Pulp and Paper Research Foundation is gratefully acknowledged.

REFERENCES

1. BROBERG, K.B., "Critical Review of Some Theories in Fracture Mechanics", *Intl. J. Fract. Mech.* 4:1–18 (1968).
2. BROBERG, K.B., Cracks and Fracture, Academic Press (1999).
3. KALLMES, O.J., "A Comprehensive View of the Structure of Paper" in Theory and Design of Wood and Fiber Composite Materials, B.A. Jaynne, Ed., Syracuse Univ. Press, Syracuse, NY, 157–175 (1972).
4. PAGE, D.H., "A Theory for the Tensile Strength of Paper", *Tappi* 5(4):674–681 (1969).
5. BITHER, T.W. and WATERHOUSE, J.F., "Strength Development Through Refining and Wet Pressing", *Tappi J.* 201– 208 (Nov. 1992).
6. BARENBLATT, G.I., "The Formation of Equilibrium Cracks During Brittle Fracture. General Ideas and Hypotheses. Axially-Symmetric Cracks", *Prikl. Math. Mekh.* 23(3):434–444 (English transl. *J. Appl. Mech.* 23:622–636) (1959).
7. ANDERSSON, H. and BERGKVIST, H., "Analysis of a Non-Linear Crack Model", *J. Mech. Phys. Solids* 18:1–28 (1970).
8. HILLERBORG, A., MODEER, M. and PETERSSON, P.E., "Analysis of Crack Formation and Crack Growth in Concrete by Means of Fracture Mechanics and Finite Elements", *Cement Concrete Res.* 6:773–782 (1976).
9. TRYDING, J., "In-plane Fracture of Paper", Doctoral Thesis, Report TVSM-1008, Lund Inst. Tech. Div. Struct. Mech., Lund, Sweden (1997).
10. TRYDING, J. and GUSTAFSSON, P.J., "Characterization of Tensile Fracture Properties of Paper", *Tappi J.* 84–89 (Feb. 2000).
11. PETERSSON, P.-E., "Crack Growth and Development of Fracture Zones in Plain Concrete and Similar Materials", Ph.D. Thesis LUTVDG/(TVBM-1006)/1981, Div. of Bld. Mat., Lund University, Lund, Sweden (1981).
12. ARONSSON, C.-G., "Tensile Fracture of Composite Laminates with Holes and Cracks", Report No 84-5, Royal Inst. Tech., Stockholm, Sweden (1984).
13. SCHELLEKENS, J.C.J., "Computational Strategies for Composite Structures", Dissertation, Delft Univ. Tech., Faculty of Civil Eng., Delft, The Netherlands (1992).
14. GUSTAFSSON, P.J., "Fracture Mechanics Studies of Non-Yielding Materials such as Concrete", Ph.D. Thesis LUTVDG/(TVBM-1007)/1985, Div. of Bld. Mat., Lund University, Lund, Sweden (1985).
15. WERNERSSON, H., "Fracture Characterization of Wood Adhesive Joints", Ph.D. Thesis LUTVDG/(TVSM-1006)/1994, Dept. Struc. Mech., Lund University, Lund, Sweden (1994).
16. GRIFFITH, A.A.,"The Phenomena of Rupture and Flow in Solids", *Phil. Trans. Royal Soc.* A221:163–198 (1920).
17. IRWIN, G.R., "Analysis of Stresses and Strains Near the End of a Crack Traversing a Plate", *J. Appl. Mech.* 24:361–364 (1957).
18. RICE, J.R., "A Path Independent Integral and the Approximate Analysis of Strain Concentration by Notches and Cracks", *J. Appl. Mech.* 35:379–386 (1968).
19. ANDERSSON, O. and FALK, O., "Spontaneous Crack Formation in Paper", *Svensk Papperstidn.* 69:91–99 (1966).
20. CHOI, D. and THROPE, J.L., "Progressive Deformation at the Crack Tip in Paper During Mode I Fracture. Part I – Bond Paper", *Tappi J.* 127–134 (Oct. 1992).
21. FELLERS, C., "Bruchzähigkeit- eine neue methode zur charakterisierung von papier", *Das Papier.* 7:345–352 (1993).
22. FELLERS, C., FREDLUND, M. and WÅGBERG, P., "Die-Cutting Toughness and Cracking of Corrugated Board", *Tappi J.* 103–109 (April 1992).
23. HELLE, T., "Fracture Mechanics of Paper" in Design Criteria for Paperperformance, P. Kolseth, C. Fellers, L. Salmén and M. Rigdahl, Eds. STFI-meddelande A 969 (1987).
24. SETH, R.S., "Measurement of In-Plane Fracture Toughness of Paper", *Tappi J.* 78(10):177–183 (1995).
25. SETH, R.S. and PAGE, D.H., "Fracture Resistance in Paper", *J. Material Sci.* 9:1745–1753 (1974).
26. SHALLHORN, P.M. , "Fracture Resistance – Theory and Experiment", *J. Pulp Paper Sci.* 20(4):119–123 (1994).
27. STEADMAN, R. and FELLERS, C., "Fracture Toughness Characterization of Paper at Different Climates", 1987 Intl. Paper Physics Conf., Mont-Rolland, QC, Canada, 173–176 (1987).
28. SWINEHART, D.E. and BROEK, D., "Tenacity, Fracture Mechanics, and Unknown Coater Web Breaks", *Tappi J.* 79(2):233–237 (1996).
29. SETH, R.S., "On the Work of Fracture in Paper", *Tappi J.* 62(7):92 (1979).
30. SETH, R.S. and PAGE, D.H., "Fracture Resistance: A Failure Criterion for Paper", *Tappi J.* 58(9):112 (1975).
31. GOLDSCHMIDT, J. and WAHREN, D., "On the Rupture Mechanism of Paper", *Svensk Papperstidn.* 71:477 (1968).
32. TRYDING, J., "A Modification of the Tsai-Wu Failure Criterion for the Biaxial Strength of Paper", *Tappi J.* 77(8):132 (1994).
33. BROBERG, K.B., "The Formulation of Fracture Mechanics", *Eng. Fracture Mech.* 16:497–515 (1982).
34. BROBERG, K.B., "Critical Review of Some Methods in Nonlinear Fracture Mechanics", *Eng. Fracture Mech.* 50:157–164 (1995).
35. OROWAN, E., "Notch Brittleness and the Strength of Metals", *Trans. Inst. Engrs. Shipbuilders, Scotland* 89:165 (1945).
36. BROBERG, K.B., "Fracture Mechanics – Theoria or Tekhne?", *Intl. J. Fracture* 57:85–99 (1992).
37. HELLAN, K., Introduction to Fracture Mechanics, MacGraw-Hill, Inc. (1984).

REFERENCE: TRYDING, J. and GUSTAFSSON, P.J., Analysis of Notched Newsprint Sheet in Mode I Fracture. Journal of Pulp and Paper Science, 27(3):103–109 March 2001. Paper offered as a contribution to the Journal of Pulp and Paper Science. Not to be reproduced without permission from the Pulp and Paper Technical Association of Canada. Manuscript received December 14, 1999; revised manuscript approved for publication by the Review Panel October 26, 2000.

KEYWORDS: NEWSPRINT, FAILURE, NOTCHES, SIMULATIONS, MODELS, CRACKS, LOADS, FRACTURE.